EasyChair Preprint

№ 2

Giant photo-effect in proton transport through graphene

Marcelo Lozada-Hidalgo, Sheng Hu, Sheng Zhang, Vasyl Kravets, Francisco J. Rodriguez, Alexey Berdyugin, Alexander Grigorenko and Andre K. Geim

September 14, 2017

Giant photo-effect in proton transport through graphene

M. Lozada-Hidalgo[1], S. Hu[2], S. Zhang[1], V. Kravets[1], F. J. Rodriguez[1], A. Berdyugin[1], A. Grigorenko[1], A. K. Geim[1]

[1]School of Physics & Astronomy and [2]National Graphene Institute, University of Manchester Manchester M13 9PL, UK

Graphene has recently been shown to be permeable to thermal protons[1], nuclei of hydrogen atoms, which sparked interest in its use as a proton-conducting membrane in relevant technologies[1-4]. Here we report that proton transport through graphene can be enhanced strongly by illuminating it with visible light. Using electrical measurements and mass spectrometry, we find a photoresponsivity of ~10^4 A W^{-1}, which translates into a gain of ~10^4 protons per photon, with response times in a microsecond range. These characteristics are competitive with those of state-of-the-art photodetectors based on electron transport using silicon and novel two-dimensional materials[5-7]. The photo-proton effect can be important for graphene's envisaged use in fuel cells and hydrogen isotope separation. Our observations can also be of interest for other applications such as light-induced water splitting, photo-catalysis and novel photodetectors.

Recent experiments have established that graphene monolayers are surprisingly transparent to thermal protons, even in the absence of lattice defects[1,2]. The proton transport through graphene was found to be thermally activated[1] with a relatively low energy barrier of about 0.8 eV. Further measurements involving hydrogen's isotope deuterium have shown that this barrier is in fact 0.2 eV higher than the measured activation energy because the initial state of incoming protons is lifted by zero-point oscillations at oxygen bonds within the proton-conducting media used in the experiments[2]. The resulting value of ~1.0 eV for the graphene barrier is somewhat lower (by at least 30%) than the values obtained theoretically for ideal graphene[1,8-11], which triggered a debate about the exact microscopic mechanism behind the proton permeation[8-13]. For example, it was recently suggested that graphene's hydrogenation could be an additional ingredient involved in the process[11]. Furthermore, it was shown experimentally that graphene's barrier for protons could be lowered quite substantially by decorating graphene with nanoparticles of catalytically-active metals such as Pt and Pd[1]. The latter observation also remains to be fully understood. Independently of fundamentals of the involved mechanisms, the high proton conductivity of graphene membranes combined with their impermeability to other atoms and molecules entices their use for various applications including fuel cell technologies and hydrogen isotope separation[1-4]. For example, it was argued that mass-produced membranes based on chemical-vapor-deposited graphene can dramatically increase efficiency and decrease the costs of heavy water production[4].

In this Letter, we describe an unexpected enhancement of proton transport through catalytically-activated[1] graphene under low-intensity illumination. The devices used in this work were made from

monocrystalline graphene obtained by mechanical exfoliation. The graphene crystals were suspended over microfabricated holes (~10 μm diameter) etched in silicon-nitride films, following the recipe reported previously[1,2]. The resulting free standing membranes were decorated on one side with Pt nanoparticles deposited using electron-beam evaporation (Fig. 1a). On the opposite side, a proton-conducting polymer (Nafion[14]) was drop cast and then contacted with a proton-containing PdH_x electrode[1]. In this setup, if a negative bias is applied to graphene, protons are injected from PdH_x into the Nafion film and then pass through the graphene membrane, evolving into H_2 on the side decorated with Pt nanopartciles[1,2]. Graphene – a mixed electron-proton conductor – acts here as both proton conducting membrane and cathode. Further details of device fabrication and electrical measurements are provided in Supplementary Information (see Supplementary Fig. 1).

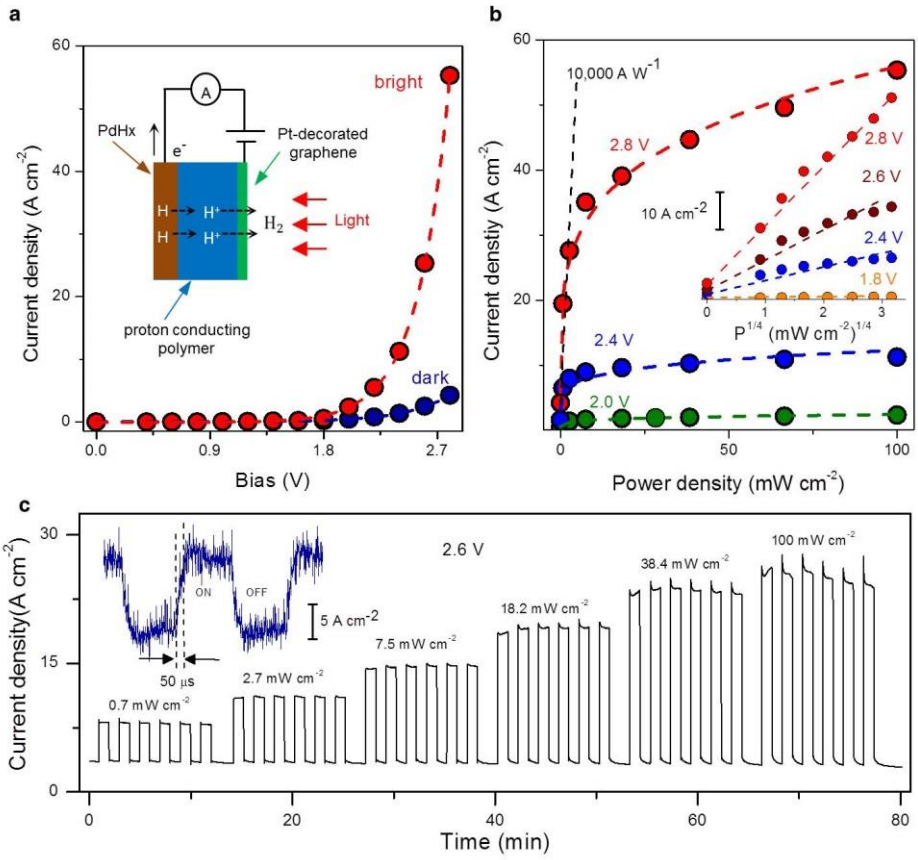

Figure 1| Influence of illumination on proton transport through graphene activated with Pt nanoparticles. a, Current-voltage characteristics for one of our devices under dark and bright conditions. Dashed curves, guides to the eye. Inset, schematic of our measurement set up. **b**, Proton current *I* as a function of illumination power *P* for different biases. Dashed curves, guides to the eye. The straight black line indicates responsivity at low illumination powers. Inset: Photo-proton effect can be described by the dependence $I \propto P^{1/4}$. **c**, Changes in *I* induced by one minute long illumination at a bias of 2.6 V; six measurements for each power density. The inset shows the frequency response found using a 1 kHz chopped illumination at 2.8 V. All the measurements were done in air.

Figure 1a shows typical current-voltage (*I-V*) characteristics of our devices measured in the dark and under simulated solar illumination of 100 mW cm^{-2} (using light source Oriel Sol3A). At zero bias, both

dark and bright currents were negligibly small. However, at higher biases (>2.0 V) where *I-V* characteristics become nonlinear, we observed that the proton current was strongly enhanced by illumination and could be ~10 times higher than the dark current. The current density (*I*) displayed a saturating dependence as a function of the illumination power density (*P*), which could be accurately described empirically using the relation $I \propto P^{1/4}$ (see Fig. 1b). At low illumination powers ($P < 5$ mW cm^{-2}), our data can also be approximated by a linear dependence on *P*, which yields a photoresponsivity of $\sim 10^4$ A W^{-1} and, probably, higher at lower intensities (<1 mW cm^{-2}) because of the nonlinear functional form *I*(*P*). For white light, this translates into a gain of $\sim 10^4$ protons per incident photon.

The photo-proton effect was also observed for graphene membranes decorated with other catalytically-active metals[15-17] such as Pd and Ni. In both cases, we observed the same power dependence $I \propto P^{1/4}$ as for Pt but the effect was somewhat weaker for both Pd and Ni (Supplementary Fig. 2). Pt and Pd are known to lower the activation energy for proton transport through graphene[1], and the same can be expected for Ni that exhibits a strong interaction with graphene[15,17]. Furthermore, if no nanoparticles were deposited on our membranes or we used nanoparticles of Au, a metal that weakly interacts with graphene[15], the proton current remained unaffected even by our strongest illumination (100 mW cm^{-2}). The latter observation shows that the photo-effect cannot be a purely plasmonic effect[18,19] or caused by heating of the device by illumination.

The exceptionally high photoresponsivity of our devices calls for their further characterization. First, we analyzed their temporal response using chopped illumination (inset of Fig. 1c). The observed changes in *I* were fast and limited by the temporal resolution of our experimental setup (Supplementary Information). This allowed only an upper bound estimate for the intrinsic response time as ≤ 50 μs. Second, using different filters we also analyzed the spectral response of the photo-proton effect. The devices displayed a flat response with no spectral features within the studied range of 450 nm to 1480 nm (Supplementary Fig. 3). Third, we determined the devices' noise equivalent power (*NEP*). This figure of merit describes the minimum radiant power measurable, taking into account the finite electric noise in the dark. To this end, we measured the noise in our devices without illumination within their operational range from 0 to 2.8 V. From these measurements, we have found a $NEP \sim 10^{-14}$-10^{-16} W Hz$^{-1/2}$ (Supplementary Fig. 4), which is an exceptionally high value.

It is instructive to compare the above characteristics due to the photo-proton effect with those of photodetectors based on electron transport. Three parameters are usually used to evaluate photodetectors: photoresponsivity, photodetectivity and response time. Let us look first at graphene and other two-dimensional crystals, materials that attract intense interest in many photo-electronic applications such as phototransistors, terahertz detectors and bolometers[5,6,20]. Without adding extra photosensitive ingredients (such as, e.g., quantum dots), graphene photodetectors typically exhibit photoresponsivities[5] ranging between ~0.1 and 100 mA W^{-1}. Other 2D crystals can exhibit a much stronger response[5,6,20]. A prominent example is monolayer MoS_2, which shows[20] a photoresponsivity of ≈880 A W^{-1} and a $NEP \sim 10^{-15}$ W Hz$^{-1/2}$, albeit with a slow rise time of ≈4 s. Another pertinent reference is commercial silicon photodiodes[7,21]. Those typically display[7,21] a photoresponsivity ~100 mA W^{-1}, a *NEP* of $\sim 10^{-12}$ W Hz$^{-1/2}$ and a response time around ~0.01-10^3 μs. In comparison, the photoresponsivity of

our devices is at least 10 times higher than the value recently highlighted for MoS_2 photodetectors[20] and 10^5 times higher than for commercial photodiodes. The response time, even though it was limited by our measurement setup, is at least 10^5 times faster than for MoS_2 and comparable to non-specialized silicon photodiodes. The third parameter, *NEP*, is comparable or higher to that of MoS_2 and commercial silicon photodetectors. This comparison suggests that the proton-based devices may be suitable for some applications even in their current non-optimized design, if all figures of merit are considered together.

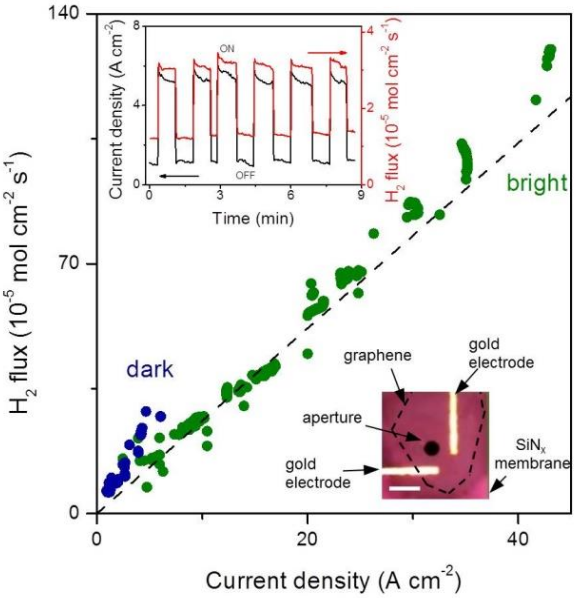

Figure 2| Photo-proton effect observed by mass spectrometry. Hydrogen flux and current density under dark and bright conditions, using biases in the range from 0 to 3 V. Dashed line: Faraday's law. Top inset: Example of raw data for simultaneously recorded I and Φ while switching illumination on and off (black curve, current; red, hydrogen flux) Bias, 2.3 V. Bottom inset: Optical image of one of our devices. The device shows two gold contacts to the graphene flake that were normally shorted. The dashed lines show the area covered with graphene. The circle in the middle is the aperture in the silicon-nitride membrane. Scale bar, 20 μm.

To gain further insight into the observed photo-proton effect, we employed another experimental approach and studied the photo-proton effect by measuring the hydrogen flux directly rather than using the electric current as a proxy. To this end, the discussed devices were placed to separate two chambers, one of which contained an H_2O/H_2 gas mixture and the other was evacuated and connected to a mass spectrometer[1,2]. The graphene membrane served as a cathode and faced the spectrometer (inset of Fig. 2). The PdHx electrode worked as an anode and faced the gas chamber. If no bias was applied or if the voltage polarity was reversed, no hydrogen flow could be detected, as expected because of graphene's impermeability to gases[1,22]. For the correct polarity, both electrical current and H_2 flow were detected and recorded simultaneously. The device worked effectively as an electrochemical pump demonstrating a 100% efficiency[1,2]. The latter means that for every two electrons that flowed through the electrical circuit an H_2 molecule appeared in the vacuum chamber. This charge-to-mass conservation is described by Faraday's law of electrolysis: $\Phi = I/2F$, where Φ is the hydrogen flux, I is the current density, F is Faraday's constant and the factor of 2 accounts for the two protons

required to form a hydrogen molecule[1,2]. In the context of this report, if the devices were illuminated at a given bias, we observed a simultaneous increase in the current density and the hydrogen flux. The Faradaic efficiency under illumination remained at 100 % (Fig. 2). These results corroborate those from our electrical measurements. It is instructive to note that, to generate a mole of hydrogen, our electrochemical pumps require the energy input $E = IV/\Phi = 2FV$, which at typical biases translates into ~50 W h per g of hydrogen.

Finally, let us discuss possible origins of the photo-proton effect. Because it requires the use of catalytically-active metals, indirect heating of graphene by illumination and plasmonic effects caused by nanoparticles can be ruled out, at least as the main reason. We also recall that Pt and Pd are known to significantly reduce the energy barrier for proton transport through graphene[1]. On this basis, we suggest that hot electrons induced by illumination in graphene transfer their energy to electrons in metal nanoparticles. This, in turn, makes the latter more catalytically reactive and lowers the barrier for proton permeation. The changes in electron temperature do not need to be massive because the proton current depends exponentially on the barrier height. This interpretation is consistent with the time scales of the processes involved. Indeed, because of strong electron-electron and weak electron-phonon coupling in graphene, its hot carriers are relatively long lived (>1 ps)[23,24]. This is to be compared with the attempt rate in proton transport, which is of the order[25,26] of 10^{13} - 10^{14} s^{-1}, that is, ~10-100 times shorter. The slow relaxation of hot electrons in graphene leads to a raised temperature of its electron gas under illumination. Indeed, the observed dependence $I \propto P^{1/4}$ is similar to that of the temperature of hot electrons in graphene, which displays a similar power law[23]. Another possible effect to consider is that the increased electron temperature can promote hydrogenation of graphene, which should also lower the proton barrier[11]. More work is needed to explain the photo-proton effect but we have to point out that the exact microscopic mechanism of proton transport through graphene is still under debate and, probably, should be understood first. On the other hand, the photo-proton effect may offer some clues for understanding the latter mechanism.

In terms of applications, the photo-proton effect also deserves some attention. The competiveness of our proton-based devices with existing and futuristic photodetectors is even more remarkable if we take into account that our devices are a first non-optimized design. For example, the addition of photosensitive materials such as quantum dots can be expected to improve their performance, as recently demonstrated for graphene-quantum-dot hybrid photodetectors based on electron transport[27]. The use of designer plasmonic nanostructures placed on top of graphene[1,2,18,19] and/or the optimization of the employed catalyst and its loading could result in further improvements. Another important application could be in fuel cells and in hydrogen isotope separation[1,3,4]. Indeed, the nonlinearity at moderate biases increases the effective proton conductivity of graphene membranes by a few orders of magnitude[1,2] (that is, above 1 S cm^{-2}); careful control of the catalyst could lead to an earlier onset of this effect. Moderate illumination would provide a further increase in the proton current by a factor of ~10, which should result in areal conductivities significantly higher than those of typical Nafion membranes used in fuel cells. The use of graphene membranes for artificial leaves[28] is yet another interesting prospect. The latter application necessitates some stringent conditions on the membranes including their mixed proton-electron conductivity, gas impermeability, mechanically stability and optical

transparency[28]. Currently, a mixture of proton and electron conducting polymers is used to satisfy those requirements, but this involves some substantial trade-offs[28]. Graphene could prove to be an interesting alternative. Most enticing, however, is probably the unexpected richness in properties and phenomena of our system where protons, electrons and photons are packed at an atomically thin interface.

1. Hu, S. *et al.* Proton transport through one-atom-thick crystals. *Nature* **516,** 227–230 (2014).
2. Lozada-Hidalgo, M. *et al.* Sieving hydrogen isotopes through two-dimensional crystals. *Science* **351,** 68–70 (2016).
3. Achtyl, J. L. *et al.* Aqueous proton transfer across single-layer graphene. *Nat. Commun.* **6,** 6539 (2015).
4. Lozada-Hidalgo, M. *et al.* Scalable and efficient separation of hydrogen isotopes using graphene-based electrochemical pumping. *Nat. Commun.* **8,** 15215 (2017).
5. Koppens, F. H. *et al.* Photodetectors based on graphene, other two-dimensional materials and hybrid systems. *Nat Nanotechnol* **9,** 780–793 (2014).
6. Lou, Z., Liang, Z. & Shen, G. Photodetectors based on two dimensional materials. *J. Semicond.* **37,** 091001 (2016).
7. Yotter, R. a. & Wilson, D. M. A review of photodetectors for sensing light-emitting reporters in biological systems. *IEEE Sens. J.* **3,** 288–303 (2003).
8. Miao, M., Nardelli, M. B., Wang, Q. & Liu, Y. First principles study of the permeability of graphene to hydrogen atoms. *Phys. Chem. Chem. Phys.* **15,** 16132–7 (2013).
9. Wang, W. L. & Kaxiras, E. Graphene hydrate: theoretical prediction of a new insulating form of graphene. *New J. Phys.* **12,** 125012 (2010).
10. Kroes, J., Fasolino, a & Katsnelson, M. Density Functional Based Simulations of Proton Permeation of Graphene and Hexagonal Boron Nitride. *Phys. Chem. Chem. Phys.* **19,** 5813–5817 (2017).
11. Feng, Y., Chen, J., Wang, E., Michelides, A. & Li, X. Hydrogenation facilitates proton transfer through two-dimensional crystals. arXiv:1704.00914 (2017).
12. Poltavsky, I., Zheng, L., Mortazavi, M. & Tkatchenko, A. Quantum tunneling of thermal protons through pristine graphene. arXiv:1605.06341 (2016).
13. Zhang, Q., Ju, M., Chen, L. & Zeng, X. C. Differential Permeability of Proton Isotopes through Graphene and Graphene Analogue Monolayer. *J. Phys. Chem. Lett.* **7,** 3395–3400 (2016).
14. Mauritz, K. & Moore, R. State of understanding of nafion. *Chem. Rev.* **104,** 4535–85 (2004).
15. Giovannetti, G. *et al.* Doping graphene with metal contacts. *Phys. Rev. Lett.* **101,** 3–6 (2008).
16. Xu, P. *et al.* Self-organized platinum nanoparticles on freestanding graphene. *ACS Nano* **8,** 2697–2703 (2014).
17. Zhou, Y. *et al.* Enhancing the hydrogen activation reactivity of non-precious metal substrates via confined catalysis underneath graphene. *Nano Lett.* **16,** 6058–6063 (2016).
18. Linic, S., Christopher, P. & Ingram, D. B. Plasmonic-metal nanostructures for efficient conversion of solar to chemical energy. *Nat. Mater.* **10,** 911–921 (2011).
19. Brongersma, M. L., Halas, N. J. & Nordlander, P. Plasmon-induced hot carrier science and technology. *Nat. Nanotechnol.* **10,** 25–34 (2015).
20. Lopez-Sanchez, O., Lembke, D., Kayci, M., Radenovic, A. & Kis, A. Ultrasensitive photodetectors based on monolayer MoS2. *Nat. Nanotechnol.* **8,** 497–501 (2013).
21. Mackowiak, V., Peupelmann, J. & Ma, Y. *ThorLabs. NEP – Noise Equivalent Power*. 5 (2016). at https://www.thorlabs.de/images/TabImages/Noise_Equivalent_Power_White_Paper.pdf (retrieved June 2017).

22. Bunch, J. S. *et al.* Impermeable atomic membranes from graphene sheets. *Nano Lett.* **8,** 2458–62 (2008).
23. Graham, M. W., Shi, S.-F., Ralph, D. C., Park, J. & McEuen, P. L. Photocurrent measurements of supercollision cooling in graphene. *Nat. Phys.* **9,** 103–108 (2013).
24. Gabor, M. *et al.* Hot carrier-assisted intrinsic photoresponse in grapahene. *Science* **334,** 648–652 (2011).
25. Marechal, Y. *The hydrogen bond and the water molecule*. (Elsevier, 2007).
26. Kreuer, K. Proton Conductivity: Materials and Applications. *Chem. Mater.* **8,** 610–641 (1996).
27. Konstantatos, G. *et al.* Hybrid graphene–quantum dot phototransistors with ultrahigh gain. *Nat. Nanotechnol.* **7,** 363–368 (2012).
28. McFarlane, S. L., Day, B. a, McEleney, K., Freund, M. S. & Lewis, N. S. Designing electronic/ionic conducting membranes for artificial photosynthesis. *Energy Environ. Sci.* **4,** 1700–1703 (2011).

Supplementary information

Device fabrication

Devices were fabricated by suspending monolayers of mechanically exfoliated graphene over apertures (≈10 μm in diameter) etched into silicon-nitride membranes (see Supplementary Figure 1). On the top side of the devices, graphene was electrically contacted using a microfabricated Au electrode patterned on the substrate prior to transferring graphene. The membranes were then decorated with a discontinuous layer of Pt or other metals (nominally ~2 nm) deposited via ebeam evaporation. The opposite side of the membrane was coated with a Nafion drop cast film (5% solution; 1100 EW) and electrically contacted with a PdH_x electrode. The whole assembly was annealed in a humid atmosphere at 130°C to crosslink the polymer. See reference 1 for further details on device fabrication.

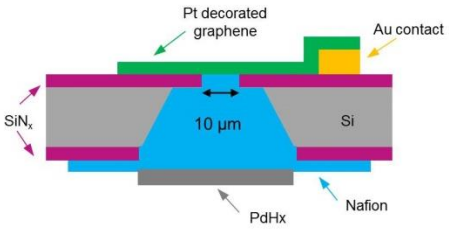

Supplementary Figure 1|Device geometry. Schematic of our devices.

Electrical measurements

For electrical measurements we measured our devices in air using a *Keithley's* sourcemeter to both apply a bias and measure current. In a typical measurement, the voltage bias was fixed and then the light was shined in one minute ON-OFF pulses. 2-6 of such pulses were shined for each voltage and illumination power density to ensure the reproducibility of the measurements. The light source was a Newport Oriel Sol3A solar simulator calibrated using the solar cell provided by the company to produce simulated solar illumination of 100 mW cm^{-2}. To obtain illumination of lower power densities we used the simulator's aperture diaphragm. This allowed us to control the intensity from 0.7 mW cm^{-2} to 100 mW cm^{-2}.

Photoresponse measurements with other metals

To gain further understanding of the photoresponse observed in our devices, we changed the metal used to decorate the graphene membranes. Supplementary Figure 2 shows the power dependence of the photoresponse in devices fabricated in the same way as the ones in the main text but with ebeam evaporated Pd or Ni instead of Pt. In panel (a) and (b) we show data of devices biased up to different voltages to show the effect at voltage ranges. Crucially, we note that both devices display the same $I \propto P^{1/4}$ response described in the main text, albeit with a somewhat (~2) smaller magnitude than with Pt. In contrast, using Au or no metal at all yielded no measurable photoresponse even under maximum illumination power density. These results, then, evidence the importance of the particular metal used to

decorate graphene and suggest the possibility of tailoring the metal catalysts' composition and loading to target different applications of the photo-proton effect.

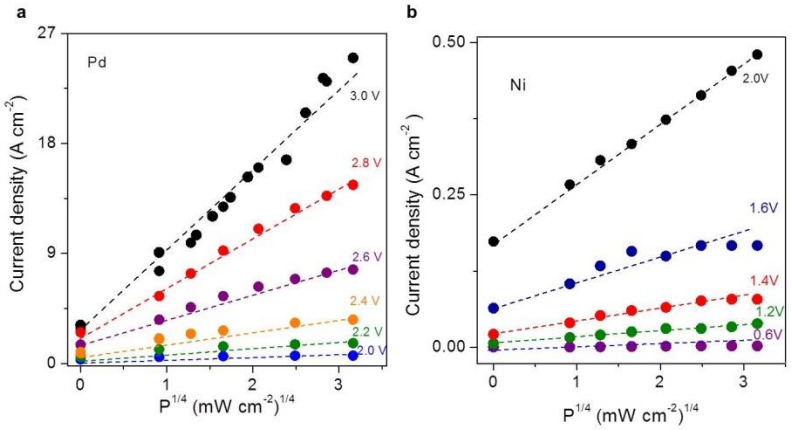

Supplementary Figure 2|Photoresponse for devices decorated with other metals. Dependence of current on illumination power density for different voltage biases. A power law, $I \propto P^{1/4}$, was observed for devices decorated with Pd (a) and Ni (b).

Spectral dependence of the photo-proton effect

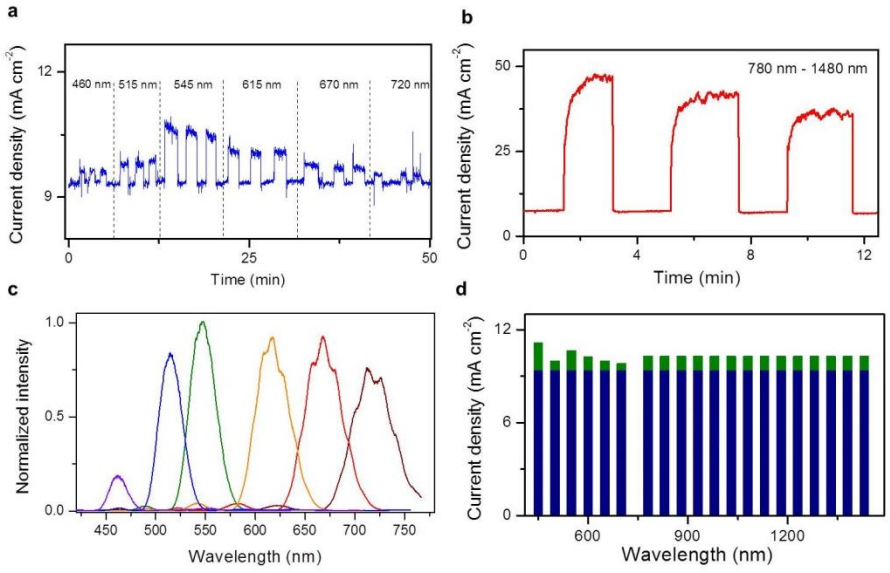

Supplementary Figure 3|Spectral dependence of photoresponse. a, Photoresponse for individual wavelengths ranging from 450-800 nm. Applied bias, 1.1 V. **b**, Three bright current pulses obtained by shining the whole 780 nm - 1480 nm range. Applied bias, 1.1 V. **c**, Optical fiber measurements of the light filtered by the liquid crystal filter over the wavelengths used in panel a. **d**, Spectral response analysis of the data in part a and b. The wavelength range from 780 to 1480 was divided in 50 nm intervals to compare with the response observed in the range 450-780. Dark current is shown in blue, bright current in green.

We studied the spectral dependence of the photoresponse of our devices in the wavelength region 450 nm - 1480 nm. To that end, a broadband laser driven white light source (Energetiq EQ-99X) was used

and different wavelength ranges were filtered. An important characteristic of this light source is that the power density is approximately flat over the entire wavelength range measured[2]. This allows for the comparison of the photoresponse of the device over different wavelengths isolated from this light source. In the 450 nm - 750 nm range, we used a liquid crystal filter to isolate individual wavelengths within a ~50 nm range, see Supplementary Figure 3c. Next, we used a short and a long pass filter to isolate the entire 780 nm - 1480 nm range from our white light source.

The photoresponse of our devices under these conditions is shown in Supplementary Figure 3 a,b. In order to compare the data from these measurements, first, we normalized the data in Supplementary Figure 3a using the relative intensity of the light filtered by the liquid crystal filter (see Supplementary Figure 3c). Next, we divided the observed photoresponse in the 780 nm – 1480 nm range between 14 intervals, each 50 nm wide. The result of this analysis is shown in Supplementary Figure 3e and shows that there are no significant spectral features in our device's photoresponse over the measured wavelength range.

Photodetector figures of merit

From our electrical measurements with solar simulated illumination it is possible to extract the photoresponsivity, R, of our devices. We extracted this parameter from the shift in current as a function of illumination power density (slope of dotted line in Figure 1b). The extracted value was $R \sim 10^4$ A W^{-1}. From these data it is also possible to estimate the maximum gain g in our devices through the relation: $g = RP/(e\phi)$ where e is the elementary charge, ϕ is the photon flux from our lamp and P is the illumination power density. Hence, from the known photon flux[3] from solar illumination at P=100 mW cm^2, $\phi \sim 10^{17}$ s^{-1} cm^{-2}, we deduce $g \sim 10^4$.

The time response of the photocurrent was measured using a broadband laser driven white light source. The light was mechanically chopped at frequencies up to 1 kHz and focused onto the device. The photocurrent values were derived from the drop in voltage through a 1 kΩ resistor connected in series with the device and the voltage source. Measurements were made with an oscilloscope and carried out with the devices in air. We note that the time response of our devices was limited by the electrical circuit's RC constant. This was shown by using different resistors and observing the corresponding change on the time constant. Thus, we can only place an upper bound to the response time as shown in the main text (≤50 μs).

In order to estimate the noise level of our devices at operational voltages, we measured the current across the device in the dark as a function of time under a fixed voltage bias ranging from 0 V to 2.8 V. To this end, the current was sampled every 100 ms during 5 minutes. Fast Fourier Transform of the measured signal was then applied to find the spectral density of current noise, S (Supplementary Figure 4). From this value, we can extract the noise equivalent power. This parameter measures the radiant power incident on the detector that produces a signal equal to the root mean square detector noise. This quantity is deduced from the spectral noise density as: $NEP=[S(f=1\text{ Hz})]^{1/2} R^{-1}$, where $S(f=1\text{ Hz})$ is the spectral noise density at 1Hz and $R \sim 10^4$ A W^{-1} is the responsivity of the devices. From our measurements, we deuced a $NEP \sim 1\text{x}10^{-14}$ W Hz$^{-1/2}$ at 2.8 V. The same measurements for small biases,

allows us to obtain the noise level floor in our devices and estimate the maximum sensitivity attainable with them. This analysis yielded a *NEP*~$1x10^{-16}$ W $Hz^{-1/2}$.

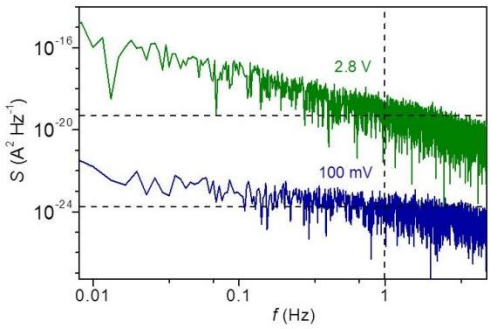

Supplementary Figure 4|Noise characterization. Current noise spectral density in the dark at fixed voltage biases.

Mass spectrometry measurements

To measure the flux of hydrogen using the mass spectrometer, each device was clamped with O-rings to separate the two chambers: one connected to a gas mixture (10% H_2 in Ar, 100% humidity) and another evacuated and connected to a mass spectrometer. The Pt layer in our devices faced the vacuum chamber; the Nafion layer, the chamber with the gas mixture. The graphene membrane was the cathode (contacted with a microfabricated Au wire; see Supplementary Figure 1) and a dc voltage *V* was applied between it and the PdH_x electrode. In this experiment the gas flow and the electric current were measured simultaneously. For the electrical measurements, a *Keithley's* SourceMeter was used both to apply the bias *V* and measure the current *I*. For the gas measurements, we used an Inficon UL200 mass spectrometer. For more details on the measurements set up, see ref. 1.

1. Hu, S. *et al.* Proton transport through one-atom-thick crystals. *Nature* **516,** 227–230 (2014).
2. http://www.energetiq.com/DataSheets/EQ99X-Data-Sheet.pdf (retrieved 2017).
3. Smestad, G. *Optoelectronics of solar cells*. (SPIE, 2002).